Optics & Laser Technology 145 (2022) 107479

Contents lists available at ScienceDirect

Optics and Laser Technology

journal homepage: www.elsevier.com/locate/optlastec

Tightly focusing vector beams containing V-point polarization singularities

Victor V. Kotlyar [a], Alexey A. Kovalev [a,*], Sergey S. Stafeev [a], Anton G. Nalimov [a], Saifollah Rasouli [b]

[a] Image Processing Systems Institute of RAS – Branch of the FSRC "Crystallography and Photonics" RAS, 151 Molodogvardeyskaya St., Samara 443001, Russia
[b] Department of Physics, Institute for Advanced Studies in Basic Sciences (IASBS), Zanjan 45137-66731, Iran

ARTICLE INFO

Keywords:
Vector beam
Polarization singularity
V-point
Tight focus
Poincare-Hopf index

ABSTRACT

We show theoretically and numerically that an n-th order vector light field containing the central V-point singularity of indefinite linear polarization with polarization singularity index n, with a 'flower' $2(n-1)$-petal polarization pattern centered on it, produces an intensity pattern with $2(n-1)$ local maxima at the tight focus. Meanwhile, a vector light field with polarization singularity index $-n$, leading to a 'web' of polarization singularities composed of $2(n+1)$ cells, is tightly focused into an intensity pattern with $2(n+1)$ intensity maxima. At the intensity nulls at the focus, either $2(n-1)$ or $2(n+1)$ V-points with alternating $+1$ or -1 indices are produced. In addition, we study more general vector fields of the order (n, m) and analytically derive their Poincare-Hopf indices for many values of n and m. Application areas of such light fields with polarization singularities are laser information technologies, laser material processing, microscopy and optical trapping.

1. Introduction

In recent years, high-order vector light fields, whose linear polarization vector varies across the beam cross-section, have been at the focus of research [1–6]. Such beams can be produced with a variety of techniques, including components with optical metasurfaces [7]. The vector beams feature a robust intensity profile on propagation through turbulence [8] and polarization singularity points [9–11] that, in many respects, are similar to phase singularity points of vortex fields [12]. Polarization singularity points (V-points) are intensity nulls in a vector field where the linear polarization vector is indefinite. The V-points are characterized [10] by a Poincare-Hopf index denoted by η, which equals the number of integer phase steps by 2π when making a full circle around the V-point. The phase is understood as the argument of a complex field composed of transverse E-field components, $E_x + iE_y$. This definition is similar to a relationship utilized in Ref. [12] to calculate the topological charge (TC) of a scalar vortex field with complex amplitude $E(x, y)$. V-points can also be characterized using a Stokes index σ, which is defined through the Poincare-Hopf index η as $\sigma = 2\eta$ and also equals the number of integer phase steps by 2π of a complex Stokes field when making a full circle around the V-point. With the unit Stokes vector $\mathbf{S} = (S_1, S_2, S_3)$ [13] having three components, the complex Stokes field is composed of the first two components: $S_c = S_1 + iS_2$. The phase of the complex Stokes field is the argument of a complex number S_c.

In this work, we derive the Poincare-Hopf and Stokes indices η and σ for n^{th}-order cylindrical vector beams. We show that in the source plane of the beams (where the on-axis field component is zero), fields of linear polarization vectors are formed centered at the V-points, which look like a 'flower' or a 'web', with the number of petals depending on the vector-field order n. Using Richards-Wolf formulae, we derive expressions for E-vector components at the tight focus for three types of vector fields, namely, for n^{th}-order radial polarization (n is positive), $-n^{\text{th}}$-order radial polarization ($-n$ is negative), and n^{th}-order azimuthal polarization. Relying on the expressions derived for the complex E-field amplitudes, we deduce expressions for transverse intensity profiles of the fields of interest. Based on the expressions derived, we obtain a major finding of this work, showing that the number of petals of the 'polarization flower' of the initial vector field equals the number of local intensity maxima at the focal plane. We also show that a V-point of an n^{th}-order vector field is 'disintegrated' at the tight focus into several first-order points with no petals around them.

2. Vector field polarization index in the source plane

Let us analyze an n^{th}-order azimuthally polarized source field whose Jones vector takes the form [14,15]:

* Corresponding author.
E-mail address: alexeysmr@mail.ru (A.A. Kovalev).

https://doi.org/10.1016/j.optlastec.2021.107479
Received 10 May 2021; Received in revised form 5 July 2021; Accepted 23 August 2021
Available online 1 September 2021

$$E_n(\varphi) = \begin{pmatrix} -sinn\varphi \\ cosn\varphi \end{pmatrix}, \quad (1)$$

where (r, φ) are the polar coordinates at the source plane. At the field center (at $r = 0$), there is a singular V-point, where the linear polarization vector is indefinite. According to Ref. [10], field (1) can be characterized by a singularity index similar to the TC of scalar optical vortices. V-points are described using a Poincare-Hopf index η, which can be calculated for field (1) similar to the TC of a complex field

$$E_{c,n}(\varphi) = E_x + iE_y = -sinn\varphi + icosn\varphi = iexp(in\varphi) \quad (2)$$

The index of field (1) and a V-point equal TC of field (2): $\eta = n$. On the other hand, vector field (1) can be characterized using Stokes parameters $\mathbf{S} = (S_1, S_2, S_3)$ [13], where

$$S_1 = \frac{|E_x|^2 - |E_y|^2}{|E_x|^2 + |E_y|^2}, \quad S_2 = \frac{2Re(E_x^* E_y)}{|E_x|^2 + |E_y|^2}, \quad S_3 = \frac{2Im(E_x^* E_y)}{|E_x|^2 + |E_y|^2}, \quad (3)$$

with Re and Im stand for the real and imaginary parts of a number. From (3), the Stokes vector is seen to be of unit length: $S_1^2 + S_2^2 + S_3^2 = 1$. For the field (1), the Stokes parameters from (3) are given by

$$S_1 = -cos(2n\varphi),\ S_2 = -sin(2n\varphi),\ S_3 = 0. \quad (4)$$

Since $S_3 = 0$ in Eq. (4), we can infer that the field (1) is linearly polarized at any point, excepting the V-point, where polarization is indefinite. The complex Stokes field for the vector (4) takes the form:

$$S_c = S_1 + iS_2 = -cos(2n\varphi) - isin(2n\varphi) = -exp(i2n\varphi) \quad (5)$$

The Stokes index for the field (1) equals TC of the field (5): $\sigma = 2\eta = 2n$. Thus, the Stokes index is twice as large as the Poincare-Hopf index.

For a radially polarized n^{th}-order field with the Jones vector

$$E_{1,n}(\varphi) = \begin{pmatrix} cosn\varphi \\ sinn\varphi \end{pmatrix} \quad (6)$$

the Poincare-Hopf index of the central V-point ($r = 0$) also equals $\eta = n$. The V-point singularity index has the opposite sign ($\eta = -n$) for a vector field

$$E_{2,n}(\varphi) = \begin{pmatrix} cosn\varphi \\ -sinn\varphi \end{pmatrix} \quad (7)$$

3. Number of local intensity maxima at the focus of a vector field

Interestingly, vector field (6) produces a 'flower'-shaped pattern of linear polarization vectors composed of $2(n-1)$ petals. Actually, a petal is inscribed between the vector found at an angle $\varphi = 0$ and the vector rotated by an angle $\varphi = \pi + \varphi_0$. From the first to the second angle, the phase of the field (6) changes by $n\varphi_0$ rad. Equating $\pi + \varphi_0 = n\varphi_0$, we find the angle for a single petal to be $\varphi_0 = \pi/(n-1)$. In total, there are N petals: $2\pi = N\varphi_0$. Hence, we find that $N = 2(n-1)$. A similar reasoning suggests that a polarization 'web' composed of linear polarization vectors around the V-point of field (7) has $N = 2(n+1)$ cells.

Next, we demonstrate that a 'flower' of linear polarization vectors composed of $2(n-1)$ petals formed by the field (6) in the source plane is transformed at the tight focus into a 'flower'-shaped intensity pattern with $2(n-1)$ local maxima.

Actually, using Richards-Wolf formulae [16], which describe the electromagnetic field components in the tight focus neighborhood, the E-field components can be derived in the form:

$$\begin{aligned} E_x &= -i^{n+1}\left(I_{0,n}cosn\varphi + I_{2,n-2}cos(n-2)\varphi\right), \\ E_y &= -i^{n+1}\left(I_{0,n}sinn\varphi - I_{2,n-2}sin(n-2)\varphi\right), \\ E_z &= 2i^n I_{1,n-1}sin(n-1)\varphi, \end{aligned} \quad (8)$$

where

$$I_{\nu,\mu} = \left(\frac{\pi f}{\lambda}\right)\int_0^{\theta_0} sin^{\nu+1}\left(\frac{\theta}{2}\right)cos^{3-\nu}\left(\frac{\theta}{2}\right) \times cos^{1/2}(\theta)A(\theta)e^{ikzcos\theta}J_\mu(x)d\theta, \quad (9)$$

where λ is the wavelength of light, f is the focal length of an aplanatic optical system, $x = krsin\theta$, $J_\mu(x)$ is the first-kind Bessel function, and $NA = \sin\theta_0$ is the numerical aperture. The initial amplitude function $A(\theta)$ (herein assumed to be real) may be either constant (a plane wave) or in the form of a Gaussian beam

$$A(\theta) = exp\left(\frac{-\gamma^2 sin^2\theta}{sin^2\theta_0}\right), \quad (10)$$

where γ is constant. The transverse intensity (without regard for the longitudinal component of the field (8)) is given by

$$I_t = |E_x|^2 + |E_y|^2 = I_{0,n}^2 + I_{2,n-2}^2 + 2I_{0,n}I_{2,n-2}cos(2(n-1)\varphi) \quad (11)$$

From (11), the transverse intensity profile is seen to have $2(n-1)$ local intensity maxima centered on the optical axis, each being located on a ray $\varphi = 2\pi p/(2n-2)$, $p = 1, 2, 3, \ldots, 2(n-1)$. Now we will determine an index of the V-point at the focus of the vector field (8). For this purpose, an equivalent complex field and its amplitude can be expressed as

$$\begin{aligned} E_{c,n} &= \left(I_{0,n}cosn\varphi + I_{2,n-2}cos(n-2)\varphi\right) \\ &\quad + i\left(I_{0,n}sinn\varphi - I_{2,n-2}sin(n-2)\varphi\right) \\ &= I_{0,n}exp(in\varphi) + I_{2,n-2}exp(-i(n-2)\varphi) \end{aligned} \quad (12)$$

In the general case, the index of the field (8) is undefined, because while at certain radii r coefficients in one exponential function can be larger than those in another one, the situation may be opposite at other radii. In the complex field of Eq. (12), TC depends on asymptotic properties of integrals (9). For instance, putting $A(\theta) = \delta(\theta - \theta_0)$, the integrals in (9) are replaced by Bessel functions, so that (12) is rearranged to

$$E_{c,n} = AJ_n(\alpha r)exp(in\varphi) + BJ_{n-2}(\alpha r)exp(-i(n-2)\varphi), \quad (13)$$

with $\alpha = kr\sin\theta_0$ and

$$A = \left(\frac{\pi f}{\lambda}\right)sin\left(\frac{\theta_0}{2}\right)cos^3\left(\frac{\theta_0}{2}\right)cos^{1/2}\theta_0,$$

$$B = \left(\frac{\pi f}{\lambda}\right)sin^3\left(\frac{\theta_0}{2}\right)cos\left(\frac{\theta_0}{2}\right)cos^{1/2}\theta_0.$$

While from (13), the index is still seen to be undefined, near the optical axis the amplitude of a lower-order Bessel function is larger than that of a higher-order Bessel function, which means that, similar to the TC of a superposition of two optical vortices [17], the near-axis index equals $\eta = -(n-2)$. In a particular case of $n = 1$ (conventional radial polarization) Eq. (12) suggests that

$$E_{c,1} = (I_{0,1} - I_{2,1})exp(i\varphi) \quad (14)$$

In this case, the V-point index is unit ($\eta = 1$) and, considering that $n = 1$, the source field index remains the same at the focus. This clearly follows from the fact that a singular point with unit index is unable to disintegrate into a number of V-points with smaller indices. In a similar way, a scalar optical vortex with TC = 1 remains robust following stochastic amplitude and phase distortions.

For an n^{th}-order azimuthally polarized vector source field of Eq. (1), $2(n-1)$ local intensity maxima will also occur at the focus, though being

Table 1
Poincare-Hopf index η of vector field (23): *n* shown on the horizontal lines and *m* – on the vertical.

m	*n*										
	0	1	2	3	4	5	6	7	8	9	10
0	0	0	0	0	0	0	0	0	0	0	0
1	0	1	0	1	0	1	0	1	0	1	0
2	0	0	2	0	0	0	2	0	0	0	2
3	0	–1	0	3	0	–1	0	–1	0	3	0
4	0	0	0	0	4	0	0	0	0	0	0
5	0	1	0	1	0	5	0	1	0	1	0
6	0	0	–2	0	0	0	6	0	0	0	–2
7	0	–1	0	–1	0	–1	0	7	0	–1	0
8	0	0	0	0	0	0	0	0	8	0	0
9	0	1	0	–3	0	1	0	1	0	9	0
10	0	0	2	0	0	0	2	0	0	0	10

located on other rays. Hence, a focal 'flower' composed of local intensity maxima will be rotated by an angle of $\pi/(2n-2)$. Using the angle magnitude, it becomes possible to distinguish n^{th}-order radial polarization from n^{th}-order azimuthal one. Meanwhile, the number of 'flower's petals' enables a cylindrical polarization order to be determined. Actually, for a source field (1), E-vector components in the focal plane take a form similar to Eq. (8):

$$\begin{aligned} E_x &= i^{n+1}\left(I_{0,n}sinn\varphi + I_{2,n-2}sin(n-2)\varphi\right),\\ E_y &= i^{n+1}\left(-I_{0,n}cosn\varphi + I_{2,n-2}cos(n-2)\varphi\right),\\ E_z &= -2i^n I_{1,n-1}sin(n-1)\varphi. \end{aligned} \tag{15}$$

For the source field (1), the transverse intensity distribution in the focus is

$$I_t = |E_x|^2 + |E_y|^2 = I_{0,n}^2 + I_{2,n-2}^2 - 2I_{0,n}I_{2,n-2}cos(2(n-1)\varphi) \tag{16}$$

From (16), $2(n-1)$ local maxima are seen to reside on a circle centered at the optical axis and on the rays outgoing from the center at angles $\varphi = (\pi + 2\pi p)/(2n-2)$, $p = 0, 1, 2, \ldots, 2n-3$. To find indices of V-points at the focal spot of the vector field (1), we can express an equivalent complex field with the amplitude:

$$\begin{aligned} E_{c,n} &= \left(I_{0,n}sinn\varphi + I_{2,n-2}sin(n-2)\varphi\right)\\ &+i\left(-I_{0,n}cosn\varphi + I_{2,n-2}cos(n-2)\varphi\right)\\ &= -iI_{0,n}exp(in\varphi) + iI_{2,n-2}exp(-i(n-2)\varphi) \end{aligned} \tag{17}$$

In the general case, the index of the field (17) is undefined, because while at certain radii r coefficients in one exponential function can be larger than those in another one, the situation may be opposite at other radii. However, at $n = 1$ (ordinary azimuthal polarization), from Eq. (17) it follows that

$$E_{c,1} = -i(I_{2,1} + I_{0,1})exp(i\varphi) \tag{18}$$

In this case, the V-point index is unit ($\eta = 1$), meaning that the index of initial field (1) remains unchanged at the focus.

A vector 'web' of source field (7) with $2(n+1)$ cells, centered on the V-point polarization singularity is transformed at the focus into an intensity pattern with $2(n+1)$ local maxima. Actually, for the source field in (7), projections of the E-vector are given by ($n > 0$)

$$\begin{aligned} E_x &= i^{n-1}\left(I_{0,n}sinn\varphi + I_{2,n+2}sin(n+2)\varphi\right),\\ E_y &= i^{n-1}\left(I_{0,n}cosn\varphi - I_{2,n+2}cos(n+2)\varphi\right),\\ E_z &= -2i^n I_{1,n+1}sin(n+1)\varphi. \end{aligned} \tag{19}$$

For the field (19), the transverse intensity distribution at the focus is given by

$$I_t = |E_x|^2 + |E_y|^2 = I_{0,n}^2 + I_{2,n+2}^2 - 2I_{0,n}I_{2,n+2}cos(2(n+1)\varphi) \tag{20}$$

From (20), the intensity distribution is seen to have $2(n+1)$ local intensity maxima at the focus on an axis-centered circle of a certain radius. Hence, the vector 'web' in the source field of Eq. (7) can be identified based on the number of petals of an n^{th}-order vector 'flower'.

Putting $n = -1$ in Eq. (7) for the source field, we may infer from (14) that the V-point index changes sign at the focus, because based on Eq. (19) for the E-vectors at the focus, we find that

$$E_{c,1} = -i(I_{2,1} + I_{0,1})exp(i\varphi) \tag{21}$$

Aiming to determine the V-point index at the focus of the vector field (7) and using Eq. (19), we form an equivalent complex field with the amplitude:

$$\begin{aligned} E_{c,n} &= \left(I_{0,n}sinn\varphi + I_{2,n+2}sin(n+2)\varphi\right)\\ &+i\left(I_{0,n}cosn\varphi - I_{2,n+2}cos(n+2)\varphi\right)\\ &= iI_{0,n}exp(-in\varphi) - iI_{2,n+2}exp(i(n+2)\varphi) \end{aligned} \tag{22}$$

Just like in Eq. (17), the index of field (19) is undefined, but like in Eq. (13), it can be asserted that at the focus the near-axis V-point index is equal to a lesser number of the Bessel function, i.e. $\eta = -n$. That is, given the source field of Eq. (7), the near-axis V-point index at the focus is the same as in the source plane.

4. Polarization singularity index for a generalized vector field

Obviously, the above reasoning cannot be automatically applied to a generalized vector field as it has different orders on the different axes. For such a field, the Jones vector is [10]

$$E_{2,n}(\varphi) = \begin{pmatrix} cosn\varphi \\ sinm\varphi \end{pmatrix} \tag{23}$$

Although the field (23) may also be said to have a central V-point, its index can be defined analytically only in some cases (see Appendix A). Actually, the complex field equivalent to the field (23) is given by

$$E_{c,n}(\varphi) = E_x + iE_y = cosn\varphi + isinm\varphi. \tag{24}$$

In the topic-related work [10], it was not specified in which way the index of such a field could be determined if $n \neq m$. In this work, we propose that the V-point index of the vector field (23) should be calculated in a similar way to calculating the TC of scalar optical vortices using the Berry's formula [12]:

$$TC = \frac{1}{2\pi}\lim_{r\to\infty} Im\int_0^{2\pi} d\varphi \frac{\partial E(r,\varphi)/\partial\varphi}{E(r,\varphi)}. \tag{25}$$

Then, according to (25), the Poincare-Hopf index for vector field (24) is given by

$$\begin{aligned} \eta &= \frac{1}{2\pi}\lim_{r\to\infty}\mathrm{Im}\int_0^{2\pi} d\varphi \frac{-nsinn\varphi + imcosm\varphi}{cosn\varphi + isinm\varphi} =\\ &\frac{1}{2\pi}\int_0^{2\pi} d\varphi \frac{nsinn\varphi sinm\varphi + mcosm\varphi cosn\varphi}{cos^2 n\varphi + sin^2 m\varphi}. \end{aligned} \tag{26}$$

From (26), it follows that at $m = n$, $\eta = n$, whereas at $m = -n$, $\eta = -n$. However, at $n \neq \pm m$, the integral in Eq. (26) is not reduced to reference integrals. In separate cases, Eq. (26) can be calculated analytically (Appendix A), but in other cases it needs to be calculated numerically.

Table 1 below gives values of η, which were calculated using Eq. (26) for vector field (23), with the orders m and n being varied from 0 to + 10 (for negative m and n, symmetry rules can be used, as is derived in Appendix A: $\eta_{-n,m} = \eta_{n,m}$ and $\eta_{n,-m} = -\eta_{n,m}$). From Table 1, polarization singularity index can be only integer. It is also interesting that at $n = 1$, –1 and any m, the η index is equal to either 1, or 0, or –1. Also, at $n = 8$, –8 and any m, the η index equals either 8, or 0, or –8. The same holds for $n = 4$ and $n = 2$.

5. Numerical modeling

Shown in Fig. 1 are source vector fields with polarization singularity (V-point) at the center for the n^{th}-order vector field (6): (a) 3, (b) 4, (c)

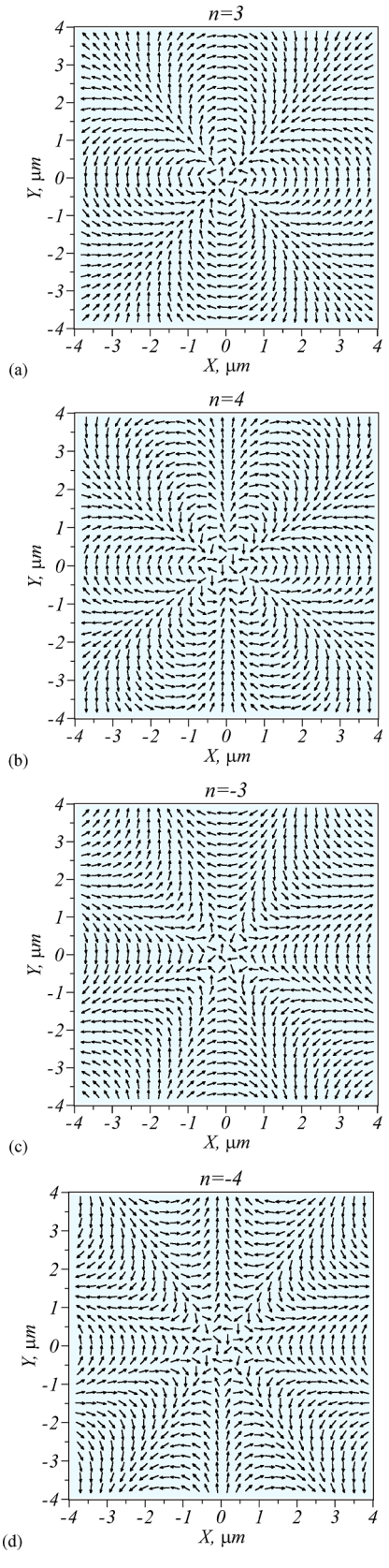

Fig. 1. Vector field (6) (arrows mark linear polarization vectors at particular points), whose order n coincides with the index of the V-point polarization singularity (Poincare-Hopf index η) at the field center and equals: (a) 3, (b) 4, (c) –3, and (d) –4.

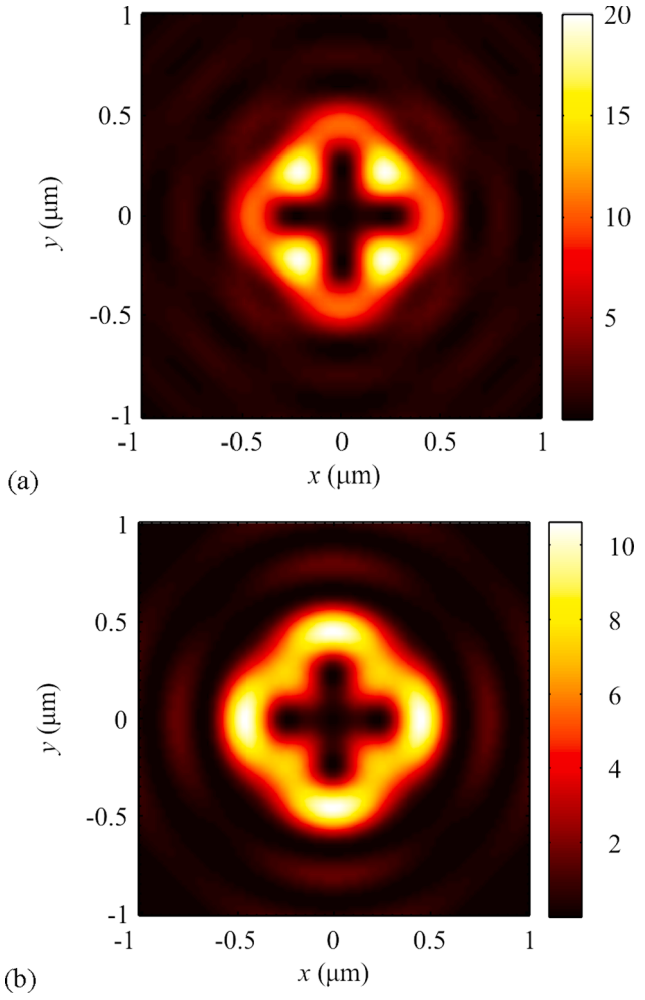

Fig. 2. Patterns of the (a) total intensity $I_x + I_y + I_z$ and (b) transverse intensity components $I_x + I_y$ from the source vector field of Fig. 1(a) at $n = 3$.

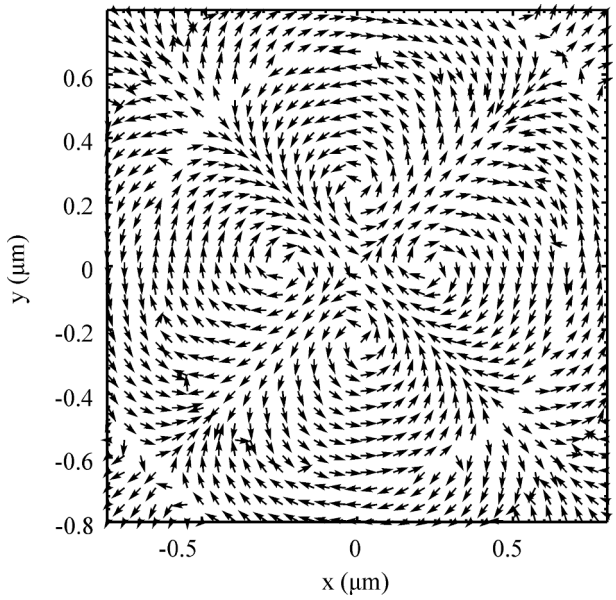

Fig. 3. Pattern of linear polarization vectors at the focal plane from the source vector field in Fig. 1(a) ($n = 3$).

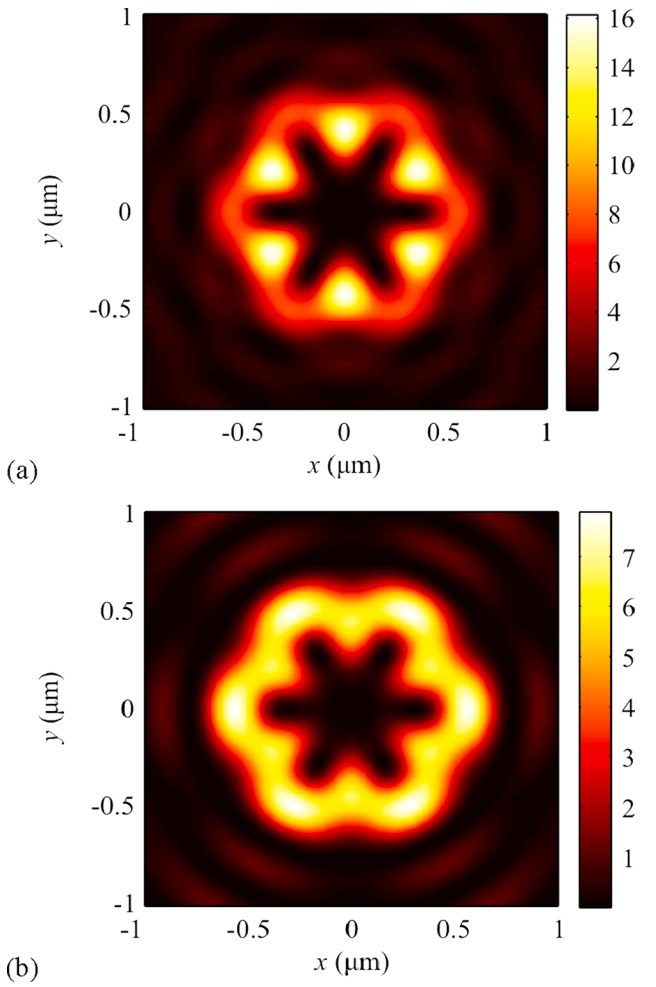

Fig. 4. Patterns of the (a) total intensity $I_x + I_y + I_z$ and (b) transverse intensity $I_x + I_y$ component at the focal plane (NA = 0.95) from the source vector field with the index $n = 4$ [Fig. 1(b)].

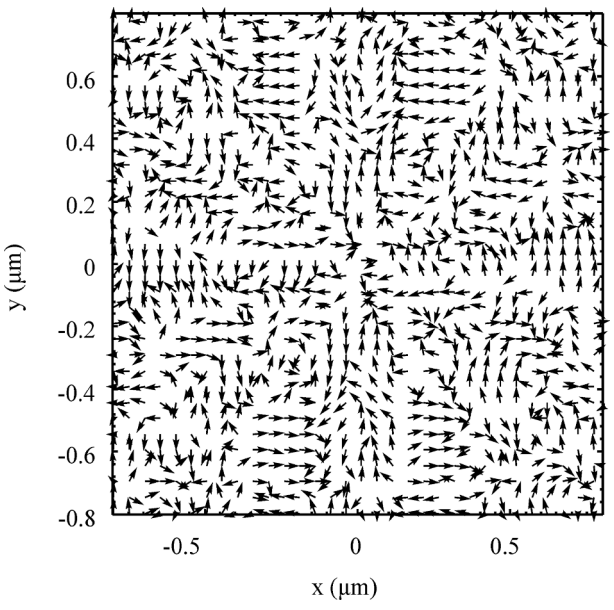

Fig. 5. Pattern of linear polarization vectors for the source vector field of Fig. 1 (b) with the index $n = 4$.

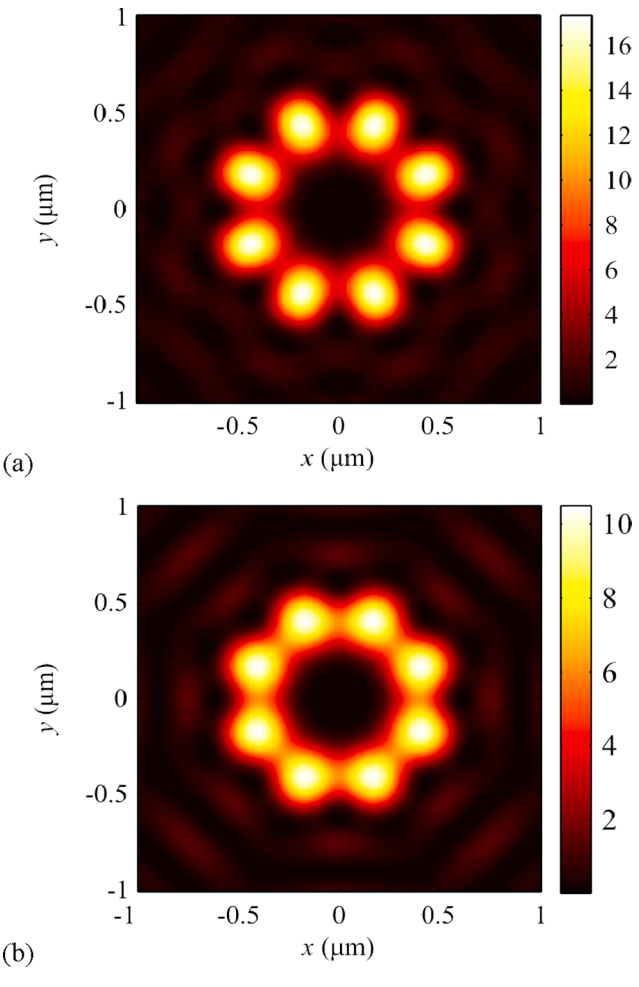

Fig. 6. Patterns of the (a) total intensity $I_x + I_y + I_z$ and (b) transverse intensity $I_x + I_y$ component at the focal plane (NA = 0.95) for the source vector field with the index $n = -3$ of Fig. 1(c).

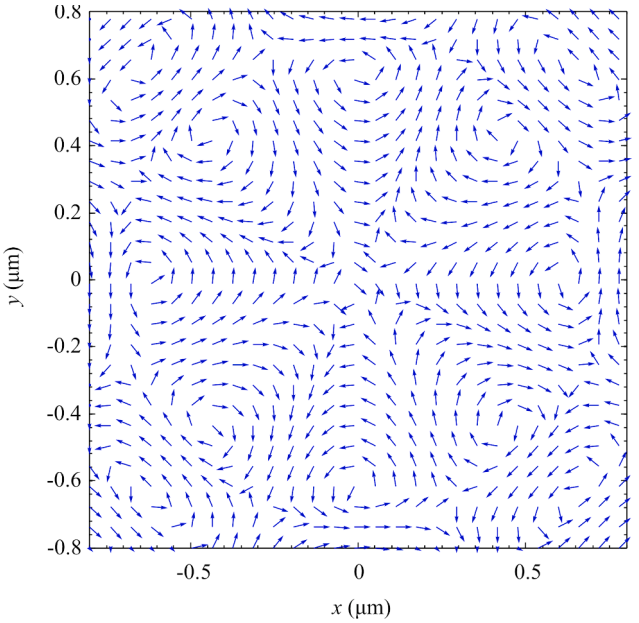

Fig. 7. Pattern of linear polarization vectors at the focus from the source field with the index $n = -3$ of Fig. 1(c).

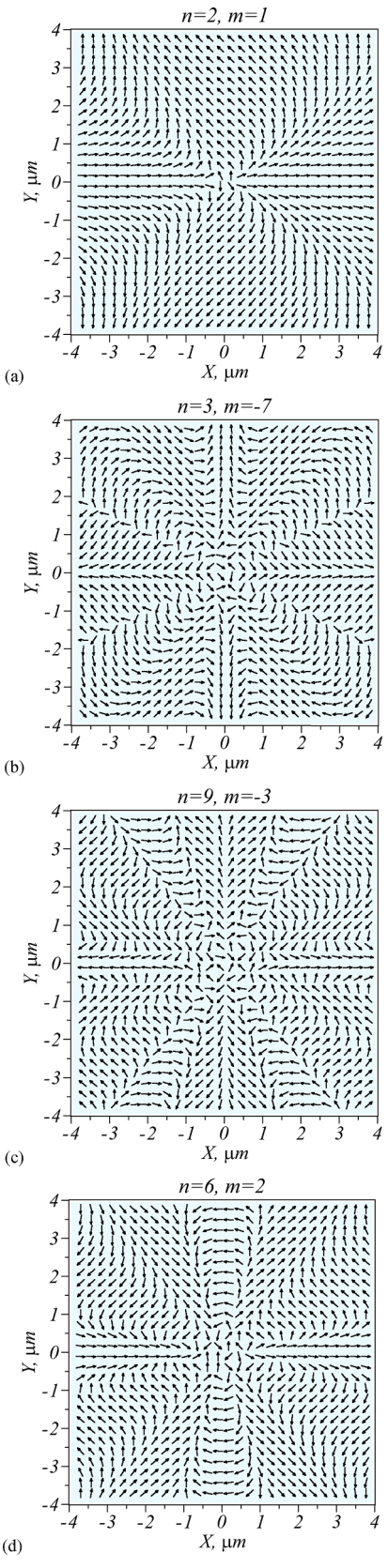

Fig. 8. Source vector fields (23) at different n and m.

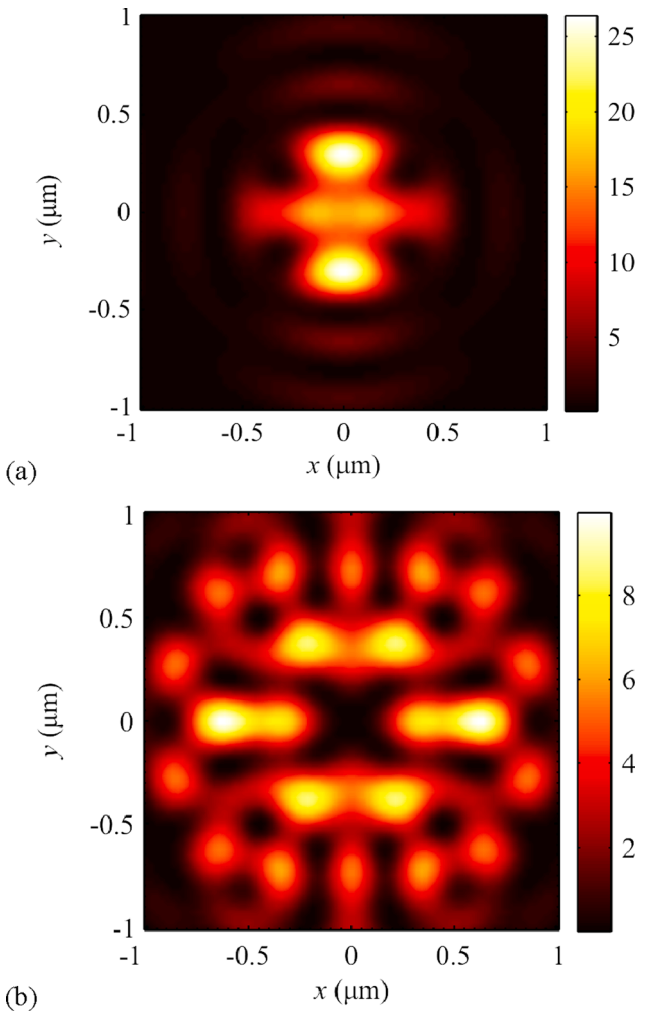

Fig. 9. Intensity patterns at the focus of vector beams with (a) $n = 2$, $m = 1$ (a 'butterfly') and (b) $n = 3$, $m = –7$ (a 'dragon mouth').

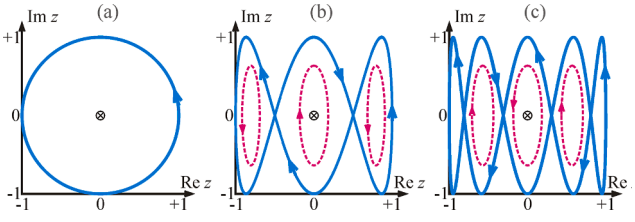

Fig. A1. Calculation of the Poincare-Hopf index. Contours Γ (blue solid curves) in the complex plane defined as $\zeta = \cos\varphi + i\,(2p+1)\sin\varphi$ $(0 \le \varphi \le 2\pi)$ for $p = 0$ (a), $p = 1$ (b), $p = 2$ (c). Red dashed ellipses show the simple contours without self-intersections, into which the contour Γ can be split. The cross in the center denotes $\zeta = 0$, the only pole of the integrand in (A6). (For interpretation of the references to colour in this figure legend, the reader is referred to the web version of this article.)

–3, and (d) –4. In compliance with the theoretical predictions, the vector fields in Fig. 1(a,b) are shaped as 'flowers' with the number of petals equal to (a) $2(n-1) = 4$ and (b) $2(n-1) = 6$. Whereas two other vector fields in Fig. 1(c,d) produce 'lattice' patterns with the number of cells equal to (c) $2(n+1) = 8$ and (d) $2(n+1) = 10$.

Source vector fields of type (6) in Fig. 1 are transformed at the focal plane into vector fields (8), (15), and (19), which have several points of polarization singularities. Shown in Fig. 2 are the total intensity [Fig. 2 (a)] and the transverse intensity [Fig. 2(b)] for a source vector field with

the index $n = 3$ of Fig. 1(a). The numerical modeling of focusing vector fields was conducted using Richards-Wolf formulae [16] for wavelength 532 nm and numerical aperture NA = 0.95.

In accordance with theoretical predictions [Eq. (11)], there occur $2(n - 1) = 4$ local maxima of the total and transverse intensities at the focus. Due to the longitudinal intensity components, the coordinates of four local maxima in Fig. 2(a) are different from those of the transverse intensity in Fig. 2(b).

Shown in Fig. 3 is a distribution of linear polarization vectors at the focus from the source vector field in Fig. 1(a) ($n = 3$).

From Fig. 3, four polarization singularity centers are seen to be located at the corners of the dark cross of Fig. 2, with an on-axis V-point with the index $\eta = -1$ located at the center. The indices of the four V-points at the corners of the dark cross (Fig. 2) are the same in magnitude but of different sign, with two vertical V-points having $\eta = +1$, and two horizontal V-points $\eta = -1$. Hence, the total near-axis index of the vector field of Fig. 3 equals that of the central V-point, i. e. $\eta = -1$. This conclusion agrees well with Eqs. (12) and (13): $\eta = -(n - 2) = -1$.

Fig. 4 depicts numerically simulated patterns for the (a) total intensity and (b) transverse intensity from the source vector field with $n = 4$ [Fig. 1(b)]. From Fig. 4, the theoretical relation (11) is again seen to be corroborated, with $2(n - 1) = 6$ local maxima in the intensity pattern found symmetrically to the optical axis being observed.

Fig. 5 shows a pattern of linear polarization vectors at the focus from a source vector field with $n = 4$ [Fig. 1(b)]. From Fig. 5, a set of V-points with indices $\eta = +1, -1$ are seen to form at the 'vertices of a dark six-point star' of Fig. 4. Equation (12) suggests that an on-axis V-point with $\eta = -2$ is found at the center.

Fig. 6 depicts patterns for the total [Fig. 6(a)] and transverse [Fig. 6(b)] component of the intensity at the focal plane (NA = 0.95) from the source vector field with $n = -3$ of Fig. 1(c). Fig. 6 shows that in compliance with theoretical predictions, there are $2(n + 1) = 8$ local intensity maxima in the intensity distribution.

Shown in Fig. 7 is a pattern of linear polarization vectors at the focus from the source vector field of Fig. 1(c) at $n = -3$. From Fig. 7, eight V-points are seen to be located on a circle (at the vertices of a 'dark eight-point star'), with four of them having the index $\eta = +1$ and four having the index $\eta = -1$. Equation (22) suggests that at the center of the focal spot there is a V-point with $\eta = 3$.

Fig. 8 presents patterns of linear polarization vectors for the source field of Eq. (23) at different values of (n, m): (a) (2,1), (b) (3,–7), (c) (9,–3), and (d) (6,2). Using the Table above, the Poincare-Hopf indices η for the said vector fields can be found to be (a) 0, (b) 1, (c) –3, and (d) 2. By looking at Fig. 8, indices of the V-points of such complex vector fields would be difficult to determine. The pattern for linear polarization vectors at the focus would be even more complicated (not presented here). Shown in Fig. 9 is an intensity pattern at the focus of an aplanatic objective with NA = 0.95 when focusing vector beams with $n = 2$, $m = 1$ [Fig. 9(a)] and $n = 3$, $m = -7$ [Fig. 9(b)].

Fig. 9 suggests that a source field with $\eta = 0$ [Fig. 8(a)] produces neither an intensity null nor a V-point at the center of the focal spot [Fig. 9(a)], whereas a source vector field with $\eta = 1$ [Fig. 9(b)] produces at the center an intensity null and a V-point.

6. Conclusions

Summing up, we have shown both theoretically and numerically that an n^{th}-order source vector field has a central V-point with the Poincare-Hopf index $\eta = n$ and the Stokes index $2n$. Such a vector field is 'flower'-shaped with $2(n - 1)$ petals. When tightly focused, this field produces at the focus an intensity pattern with $2(n - 1)$ local maxima located on a circle of certain radius, centered on the optical axis. Near those intensity maxima, $2(n - 1)$ local minima are found (intensity nulls, polarization singularity points), where V-point singularities with alternating indices $+1$ and -1 (the total index being zero) are located. An intensity null, or a V-point with the index $-(n - 2)$, has also been shown to occur at the center of the focus.

It has also been shown that an $-n^{th}$-order source vector field has at the center a V-point with the index $-n$. Such a vector field is in the form of a 'web' with $2(n + 1)$ cells. At the tight focus, this field produces an intensity pattern with $2(n + 1)$ local maxima located on a circle of certain radius centered on the optical axis. Near those intensity maxima, $2(n + 1)$ local minima are found (intensity nulls, polarization singularity points), where V-points with alternating indices $+1$ and -1 (the total index being zero) are located. An intensity null, or a V-point with the index $-n$, has also been shown to occur at the center of the focus. For an (n, m)-order vector field, indices of V-points (see the Table) have been numerically calculated for the numbers varying from –10 to + 10. For a number of cases, indices of a generalized vector field have been derived analytically (Appendix A).

Such vector fields with V-point singularities can be generated experimentally by using either q-plates, i.e. specially transversely patterned liquid crystal cells inducing an integer or semi-integer topological charge [18,19], or, for higher Poincare-Hopf indices, by spatial light modulators: either by one, with double modulation technique [20], or by two [21].

Application areas of such light fields with polarization singularities are laser information technologies [22], laser material processing [23], microscopy [24] and particle manipulation or optical trapping [25].

CRediT authorship contribution statement

Victor V. Kotlyar: Conceptualization, Methodology, Formal analysis, Writing – original draft, Funding acquisition, Writing – review & editing, Supervision. **Alexey A. Kovalev:** Methodology, Formal analysis, Investigation. **Sergey S. Stafeev:** Formal analysis, Funding acquisition, Validation, Software, Visualization. **Anton G. Nalimov:** Software, Writing – review & editing, Visualization. **Saifollah Rasouli:** Validation, Writing – review & editing.

Declaration of Competing Interest

The authors declare that they have no known competing financial interests or personal relationships that could have appeared to influence the work reported in this paper.

Acknowledgements

The work was partly funded the Russian Foundation for Basic Research under grant #18-29-20003 (in part "Polarization singularity index of the vector field in the initial plane"), the Russian Science Foundation grant #18-19-00595 (in part "The number of local intensity maxima in the focus of the vector field") and by the RF Ministry of Science and Higher Education within a state contract with the "Crystallography and Photonics" Research Center of the RAS (in part "Simulation").

Appendix A. . Calculating polarization singularity index of a generalized vector field

Below, we deduce some properties of polarization singularity index (26), including properties of parity, symmetry, reciprocity, and multiplicity.

The parity property is expressed in the fact that for different-parity m and n (i.e. $m + n$ is odd), polarization singularity index (26) equals zero. Actually, the first integral in (26) can be broken down in two (with the range of integration in the second integral shifted from $[\pi, 2\pi]$ to $[0, \pi]$):

$$\eta_{n,m}=\frac{1}{2\pi}\mathrm{Im}\{\int_0^{\pi}\frac{-n\sin n\varphi+im\cos m\varphi}{\cos n\varphi+i\sin m\varphi}d\varphi + \int_0^{\pi}\frac{-n(-1)^n\sin n\varphi+im(-1)^m\cos m\varphi}{(-1)^n\cos n\varphi+i(-1)^m\sin m\varphi}d\varphi\} \tag{A1}$$

Multiplying the numerator and denominator of the first integral by $(-1)^n$ and taking into account that $(-1)^{m+n}=-1$, we get a sum of two complex conjugated numbers whose imaginary part equals zero.

Thus, we obtain a symmetry property of the Poincare-Hopf index for vector field (23). In this way, it stands to reason that when n changes sign, the first integral in (26) does not change:

$$\eta_{-n,m}=\frac{1}{2\pi}Im\int_0^{2\pi}d\varphi\frac{-(-n)\sin(-n\varphi)+im\cos m\varphi}{\cos(-n\varphi)+i\sin m\varphi}=\eta_{n,m}. \tag{A2}$$

On the contrary, when m changes sign, the integrand becomes complex conjugated and, hence, the imaginary part changes sign:

$$\eta_{n,-m}=-\eta_{n,m.} \tag{A3}$$

Shifting the range of integration by $\pi/2$, we get the following relationships between the indices:

$$\eta_{n,m}=\begin{cases}\dfrac{1}{2\pi}Im\displaystyle\int_0^{2\pi}d\varphi\frac{-n(-1)^{\frac{n}{2}}\sin n\varphi+im(-1)^{\frac{m}{2}}\cos m\varphi}{(-1)^{\frac{n}{2}}\cos n\varphi+i(-1)^{\frac{m}{2}}\sin m\varphi}, \\ \qquad\text{if } n,m \text{ are even,} \\ \dfrac{1}{2\pi}Im\displaystyle\int_0^{2\pi}d\varphi\frac{-n(-1)^{\frac{n-1}{2}}\cos n\varphi+im(-1)^{\frac{m+1}{2}}\sin m\varphi}{(-1)^{\frac{n+1}{2}}\sin n\varphi+i(-1)^{\frac{m-1}{2}}\cos m\varphi}, \\ \qquad\text{if } n,m \text{ are odd,}\end{cases} \tag{A4}$$

$$=\begin{cases}(-1)^{(m-n)/2}\eta_{n,m}, & \text{if } n,m \text{ are even,}\\ (-1)^{(m-n)/2}\eta_{m,n}, & \text{if } n,m \text{ are odd.}\end{cases}$$

This can be termed as a reciprocity property because it enables the indices to be swapped if they are odd.

From (A4), it also follows that if n and m are even, but $(m-n)/2$ is odd, then $\eta=0$.

If the orders m and n have a common divisor, i.e. $m=p\mu$ and $n=p\nu$, then, performing a change of variables $\varphi=\theta/p$ in (26), we obtain a multiplicity property:

$$\eta_{p\nu,p\mu}=p\frac{1}{2\pi}\mathrm{Im}\int_0^{2\pi p}\frac{-\nu\sin\nu\theta+i\mu\cos\mu\theta}{\cos\nu\theta+i\sin\mu\theta}\frac{d\theta}{p}=p\eta_{\nu,\mu}. \tag{A5}$$

For instance, at $m=2n$, polarization singularity index equals zero thanks to the multiplicity and parity properties: $\eta_{n,2n}=n\eta_{1,2}=0$.

In a simple case, we determine the index $\eta_{1,2p+1}$ analytically through the use of residues. If we denote $\zeta=\cos\varphi+i(2p+1)\sin\varphi$, the integral (26) can be written as (at $n=1$)

$$\eta=\frac{1}{2\pi}\mathrm{Im}\oint_\Gamma\frac{d\zeta}{\zeta}, \tag{A6}$$

where Γ is the oriented closed contour in the complex plane drawn by the variable ζ, when $0\le\varphi\le2\pi$. Fig. A1 illustrates this contour for $p=0$, 1, 2.

If $p=0$, this contour is a simple unit-radius circle. Otherwise, Γ has self-intersections and the integral over Γ can be replaced by a sum of the integrals over several simple contours without the self-intersections [red dashed contours in Fig. A1(b,c)]. The only pole of the integrand in (A6) is $\zeta=0$. If $p=0$, this pole is within the unit-radius circle and, according to the residues theorem, applied to the integral (A6), $\eta_{11}=1$. For $p>0$, only one simple contour contains the pole [Fig. A1(b,c)]. Thus, integration over the other simple contours yields 0. If $p=1$ (and at other odd p), the pole is bypassed clockwise and, therefore, the integration yields $\eta_{13}=-1$. Similarly, if $p=2$ (and at other even p), the pole is bypassed counterclockwise and, therefore, the integration yields $\eta_{15}=+1$. Thus, we can write a general rule for the Poincare-Hopf index η_{nm} at $n=1$ and odd m:

$$\eta_{1m}=(-1)^{(m-1)/2} \tag{A7}$$

or, using the reciprocity property:

$$\eta_{n,1}=1. \tag{A8}$$

All the properties of index (26) for field (23) derived herein can be verified using the Table.

References

[1] Z. Liu, Y. Liu, Y. Ke, Y. Liu, W. Shu, H. Luo, S. Wen, Generation of arbitrary vector vortex beams on hybrid-order Poincare sphere, Photon. Res. 5 (2017) 15–21, https://doi.org/10.1364/PRJ.5.000015.

[2] S. Fu, Y. Zhai, T. Wang, C. Yin, C. Gao, Tailoring arbitrary hybrid Poincare beams through a single hologram, Appl. Phys. Lett. 111 (2017), 211101, https://doi.org/10.1063/1.5008954.

[3] Y. Zhang, P. Chen, S. Ge, T. Wei, J. Tang, W. Hu, Y. Lu, Spin-controlled massive channels of hybrid-order Poincare sphere beams, Appl. Phys. Lett. 117 (2020), 081101, https://doi.org/10.1063/5.0020398.

[4] J. Liu, X. Chen, Y. He, L. Lu, H. Ye, G. Chai, S. Chen, D. Fan, Generation of arbitrary cylindrical vector vortex beams with cross-polarized modulation, Res. Phys. 19 (2020) 103455, https://doi.org/10.1016/j.rinp.2020.103455.

[5] G. Arora, S. Deepa, S.N. Khan, P. Senthilkumaran, Detection of degenerate Stokes index states, Sci. Rep. 10 (2020) 20759, https://doi.org/10.1038/s41598-020-77365-8.

[6] G. Arora, Ruchi, and P. Senthilkumaran, "Hybrid order Poincare spheres for Stokes singularities," Opt. Lett. 45 (2020) 5136–5139. https://doi.org/10.1364/OL.400946.

[7] S.S. Stafeev, V.V. Kotlyar, A.G. Nalimov, M.V. Kotlyar, L. O'Faolain, Subwavelength gratings for polarization conversion and focusing of laser light, Phot. Nanostruct. Fundam. Appl. 27 (2017) 32–41, https://doi.org/10.1016/j.photonics.2017.09.001.

[8] P. Lochab, P. Senthilkumaran, K. Khare, Designer vector beams maintaining a robust intensity profile on propagation through turbulence, Phys. Rev. A 98 (2018), 023831, https://doi.org/10.1103/PhysRevA.98.023831.

[9] M. Berry, Geometry of phase and polarization singularities illustrated by edge diffraction and the fides, Proc. SPIE 4403 (2001).

[10] I. Freund, Polarization singularity indices in Gaussian laser beams, Opt. Commun. 201 (4-6) (2002) 251–270, https://doi.org/10.1016/S0030-4018(01)01725-4.

[11] A.A. Kovalev, V.V. Kotlyar, Gaussian beams with multiple polarization singularities, Opt. Commun. 423 (2018) 111–120, https://doi.org/10.1016/j.optcom.2018.04.023.

[12] M V Berry, Optical vortices evolving from helicoidal integer and fractional phase steps, J. Opt. A Pure Appl. Opt. 6 (2) (2004) 259–268, https://doi.org/10.1088/1464-4258/6/2/018.

[13] M. Born, E. Wolf, Principles of optics, Pergamon Press, Oxford, 1968.

[14] Q. Zhan, Cylindrical vector beams from mathematical concepts to applications, Adv. Opt. Photon. 1 (2009) 1–57, https://doi.org/10.1364/AOP.1.000001.

[15] V.V. Kotlyar, S.S. Stafeev, A.A. Kovalev, Sharp focusing of a light field with polarization and phase singularities of an arbitrary order, Computer Optics 43 (2019) 337–346, https://doi.org/10.18287/2412-6179-2019-43-3-337-346.

[16] B. Richards, E. Wolf, Electromagnetic Diffraction in Optical Systems. II. Structure of the Image Field in an Aplanatic System, in: Proceedings of the Royal Society A 253, 1959, pp. 358–379, https://doi.org/10.1098/rspa.1959.0200.

[17] V.V. Kotlyar, A.A. Kovalev, A.V. Volyar, Topological charge of a linear combination of optical vortices topological competition, Opt. Exp. 28 (2020) 8266–8281, https://doi.org/10.1364/OE.386401.

[18] F. Cardano, E. Karimi, S. Slussarenko, L. Marrucci, C. de Lisio, E. Santamato, Polarization pattern of vector vortex beams generated by q-plates with different topological charges, Appl. Opt. 51 (2012) C1–C6, https://doi.org/10.1364/AO.51.0000C1.

[19] F. Cardano, E. Karimi, L. Marrucci, C. de Lisio, E. Santamato, Generation and dynamics of optical beams with polarization singularities, Opt. Express 21 (2013) 8815–8820, https://doi.org/10.1364/OE.21.008815.

[20] P. Kumar, S. Pal, N. Nishchal, P. Senthilkumaran, Non-interferometric technique to realize vector beams embedded with polarization singularities, J. Opt. Soc. Am. A 37 (2020) 1043–1052, https://doi.org/10.1364/JOSAA.393027.

[21] B. Khajavi, E.J. Galvez, High-order disclinations in space-variant polarization, J. Opt. 18 (8) (2016) 084003, https://doi.org/10.1088/2040-8978/18/8/084003.

[22] L. Lu, Z. Wang, Y. Cai, Propagation properties of phase-locked radially-polarized vector fields array in turbulent atmosphere, Opt. Express 29 (2021) 16833–16844, https://doi.org/10.1364/OE.427003.

[23] M. Meier, V. Romano, T. Feurer, Material processing with pulsed radially and azimuthally polarized laser radiation, Appl. Phys. A 86 (3) (2007) 329–334, https://doi.org/10.1007/s00339-006-3784-9.

[24] P. Meng, S. Pereira, P. Urbach, Confocal microscopy with a radially polarized focused beam, Opt. Express 26 (2018) 29600–29613, https://doi.org/10.1364/OE.26.029600.

[25] L. Carretero, P. Acebal, S. Blaya, Three-dimensional analysis of optical forces generated by an active tractor beam using radial polarization, Opt. Express 22 (2014) 3284–3295, https://doi.org/10.1364/OE.22.003284.